Journal of Sound and Vibration 329 (2010) 415–424

Contents lists available at ScienceDirect

Journal of Sound and Vibration

journal homepage: www.elsevier.com/locate/jsvi

Spectrum of the sound produced by a jet impinging on the gas–water interface of a supercavity

A.W. Foley [a], M.S. Howe [a,*], T.A. Brungart [b]

[a] Boston University, College of Engineering, 110 Cummington Street, Boston, MA 02215, USA
[b] Applied Research Laboratory, The Pennsylvania State University, State College, PA 16804, USA

ARTICLE INFO

Article history:
Received 17 April 2009
Received in revised form
23 September 2009
Accepted 24 September 2009
Handling Editor: P. Joseph
Available online 22 October 2009

ABSTRACT

An analysis is made of the sound generated by the impingement of an air jet on the gas–water interface of a supercavity. The water is in uniform low Mach number motion over the interface. The interface is rippled by the jet, which produces an unsteady surface force on the water that behaves as a dipole or monopole acoustic source, respectively, at high and low frequencies. In a first approximation the very large difference in the gas density and that of water implies that the surface force is similar to that occurring when a jet impinges on a rigid wall. Data from recent measurements by Foley (2009, Ph.D. Dissertation, Department of Mechanical Engineering, Boston University) of the frequency spectrum of the surface force produced by the impact of a turbulent jet on a wall are used to formulate an analytical representation of the spectrum and thence to predict the sound produced in water when the same jet impinges on the cavity interface. The prediction is used to estimate the characteristics of gas jet impingement noise for an experimental supercavitating vehicle in use at the Applied Research Laboratory of Penn State University.

© 2009 Elsevier Ltd. All rights reserved.

1. Introduction

High-speed forward motion of an underwater vehicle can be realised by enclosing the vehicle over most of its length within a gaseous *supercavity*. The cavity is formed to the rear of a specially designed nose (the 'cavitator') and *ventilated* by the steady injection of gas from sources just aft of the cavitator [1–3]. Careful control of the injection rate ensures that the cavity is maintained in a stable state and continues to enclose most of the vehicle [4,5].

Navigation and control of a supercavitating vehicle usually involves the use of high frequency acoustic sensors in the nose. It is therefore important to understand and quantify the sources of noise that might degrade the guidance system. Possible sources include large scale instabilities of the cavity that influence cavity break-up at its downstream terminus, and cavity pulsations caused by over-pressurising the cavity [2]. However, it is more likely that smaller scale instabilities, with length scales smaller than the radius of the cavity, are more significant at higher frequencies and then constitute the dominant hydroacoustic noise sources [6–8]. These are associated with turbulence and bubbles in the flow along the gas–water interface, with vorticity shed from the trailing edge of the cavitator, and with the impingement of the ventilating gas on the cavity interface.

It is believed that an important component of the noise is attributable to gas impingement [9,10]. A supercavitating vehicle specially constructed at the Penn State Applied Research Laboratory (ARL) to study this mechanism is depicted

* Corresponding author.
E-mail address: mshowe@bu.edu (M.S. Howe).

0022-460X/$ - see front matter © 2009 Elsevier Ltd. All rights reserved.
doi:10.1016/j.jsv.2009.09.033

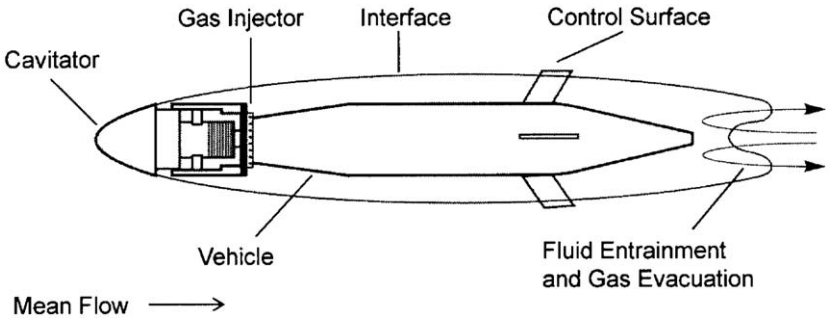

Fig. 1. Schematic of the ARL experimental supercavity.

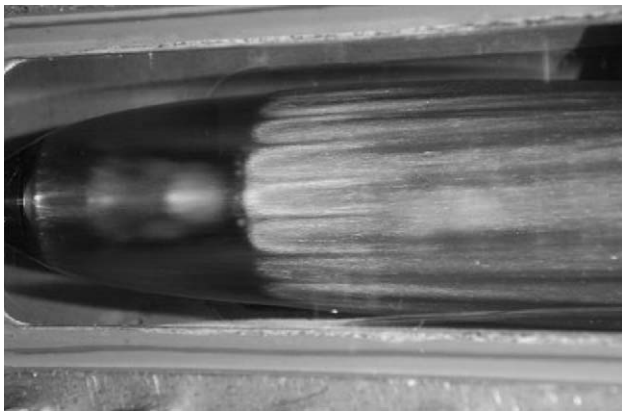

Fig. 2. Photograph of a supercavity interface rippled by radially directed jets. The flow is from left to right, and the rear end of the cavitator is just visible on the left.

schematically in Fig. 1. In a conventional supercavity gas emerging from inlet nozzles is redirected by a deflector that causes it to flow roughly parallel to the vehicle body and to strike the interface at a shallow angle. For the vehicle shown in Fig. 1, however, the deflector has been removed and gas from each nozzle forms a jet that impinges directly on the interface at close to normal incidence. There are 20 radially orientated nozzles equally spaced on a 'gas injector ring' just behind the cavitator, so that the gas enters the cavity in a closely axisymmetric sheet spanned by the jets. This arrangement is convenient because it not only promotes the production of sound by the direct impact of the jets on the gas–water interface, but also provides a geometrically simple configuration for analytical modelling.

The normally impinging jets ripple the gas–water interface in the manner illustrated in Fig. 2, which shows how each jet produces a trough-like wake on the interface in the form of a longitudinal surface depression of the water. These troughs extend far downstream in a stable configuration essentially because the gas–water interface is force-free except within the jet impact region. In practice the jet is fully turbulent so that the impact force is unsteady and forms an acoustic source that radiates into the water whose properties depend on the spectral content of the force.

Because the jet speed on impact does not normally exceed about 60 m/s, and because of the very large density difference between gas and water, it can be argued in a first approximation that for the purpose of estimating the impact forces it is permissible to treat the interface as a *rigid* surface. The impact force and pressure spectra may then be identified with those for the same jet impinging on a rigid surface of the same shape, and determined experimentally from measurements of the surface force and pressure. Foley [11] has investigated the consequences of this analogy using measurements of the surface force on a *plane* rigid wall. Predictions for this case should be applicable to the sound generated by a jet impinging normally on the supercavity interface provided the nominal diameter D of the jet impact region on the interface is smaller than the smallest radius of curvature of the interface.

Previous investigations of the production of sound by jet impingement on a rigid wall have not included measurements of surface force (see e.g. [12–16]), because for a large, plane, rigid surface the radiation is actually equivalent to that produced by a much weaker *quadrupole* source [8,15,16]. However, Strong et al. [17] have made measurements of the space–time correlation of the wall pressure on the region of a flat plate wetted by an air jet impinging at various angles of incidence. Their results for the wall pressure frequency spectrum within the impact region of a normally incident jet are compared in this paper with Foley's [11] measurements of the force spectrum.

The mathematical problem of sound generation by a jet incident on the gas–water interface is discussed in Section 2. Analytical representations of the sound radiated into the water are obtained for high, low and intermediate frequency ranges. These correspond, respectively, to the three cases where the acoustic wavelength is (i) small compared to all relevant dimensions of the cavity, (ii) large compared to the cavity length, and (iii) larger than the cavity cross-section but smaller than the overall cavity length. An empirical model is introduced in Section 3 to represent Foley's [11] data for the force spectrum; additional support for this model is provided by the earlier measurements by Strong et al. [17] of the wall pressure spectrum at the centroid of the jet impact region. Theoretical predictions are then made (Section 4) of the sound generated in the water, and a formula is proposed that defines the acoustic power spectrum at all frequencies.

2. Theory of sound generation

Gas enters the experimental supercavity of Fig. 1 in an axisymmetric fashion through a system of 20 small nozzles evenly distributed around the gas-injector ring. The jet from each nozzle is turbulent and impinges at near normal incidence on the cavity interface S. The unsteady forces exerted on S by different jets are statistically independent, and accordingly form a set of uncorrelated acoustic sources radiating into the water. It is therefore sufficient to consider the production of sound by a single jet. The spectrum of the overall far-field sound generated by all of the jets can then be obtained by simple addition of the individual spectra.

Let R be the smaller of the two principal radii of curvature of the interface S in the neighbourhood of the jet impact region. It is evident from Fig. 2 that R is large compared to the diameter D of the impact area. Therefore, the characteristics of the surface force and pressure produced by each jet must be essentially the same as for a jet impinging on a *locally plane* gas–water interface. Similarly, further simplification is possible by confining attention to those components of the sound with wavelengths larger than D. Then the calculations can be performed for the ideal case of an impinging jet of infinitesimal cross-sectional area. This approximation will certainly account for the dominant contributions to the surface generated sound, but at very high frequencies the predictions will provide only an upper bound on the acoustic intensity, because it may then actually be necessary to take into account destructive cancellation of the surface pressure sources arising from retarded time variations across the impact region of the jet [8].

2.1. Integral representation of the sound

To fix ideas, let the locally plane jet-impact region of the interface S coincide with the plane $x_3 = 0$ of the rectangular coordinate system $\mathbf{x} = (x_1, x_2, x_3)$, such that the water of density ρ_o and sound speed c_o lies in $x_3 > 0$ (Fig. 3). The Mach number of the water flowing over the interface is in practice sufficiently small that the convection of sound by the mean flow can be neglected. Small amplitude fluctuations in the pressure $p(\mathbf{x}, t)$ in the water may therefore be taken to satisfy

$$\left(\frac{1}{c_o^2}\frac{\partial^2}{\partial t^2} - \nabla^2\right) p = 0, \tag{1}$$

where t denotes time, c_o is the speed of sound in water, and possible turbulence sources of 'noise' within the flow are ignored [8].

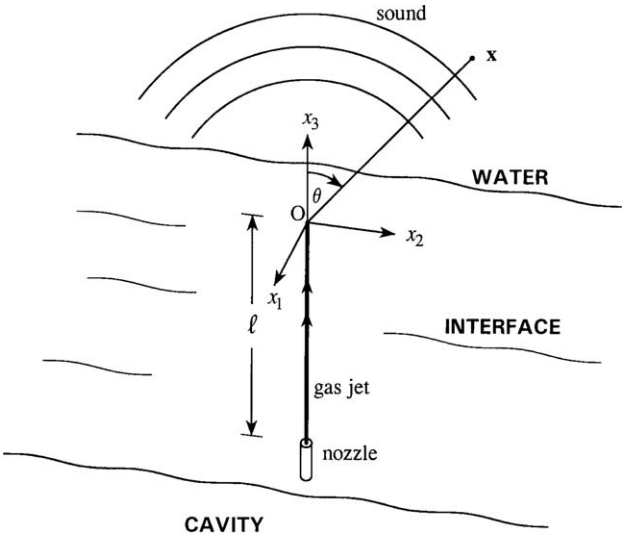

Fig. 3. Configuration of a gas jet of infinitesimal cross-section impinging on a plane interface.

The gas jet is assumed to have circular cross-section and to be coaxial with the x_3- axis and impinges at normal incidence on the interface from within the cavity where $x_3<0$. The jet exhausts at mean speed U_o from a circular nozzle of diameter D_o whose exit plane is at $x_3=-\ell$ (where $D_o\ll\ell<R$). The unsteady force $F(t)$, say, exerted on S by the jet is distributed over a circular region of the x_1x_2-plane centered on the origin and of nominal effective diameter $D\ll\ell$. This force excites unsteady motions and pressure fluctuations within the water. When attention is confined to the motions induced at distances $|\mathbf{x}|\gg D$ and when, in addition, the relevant acoustic wavelengths are much larger than D, the force $F(t)$ may be assumed to be concentrated at the origin and to correspond to a singular distribution of applied surface pressure on S equal to $F(t)\delta(x_1)\delta(x_2)$. Furthermore, the very large differences in the mean gas and water densities imply that to an excellent approximation pressure fluctuations occurring elsewhere on S can be ignored (for further discussion of this approximation see [18]). The solution of Eq. (1) should therefore represent an outgoing acoustic wave in the water subject to the condition

$$p=F(t)\delta(x_1)\delta(x_2)\quad\text{on S.}\tag{2}$$

The boundary value problem for p is solved by introducing a Green's function $G(\mathbf{x},\mathbf{y},t-\tau)$ that vanishes when either of $\mathbf{x}$, $\mathbf{y}$ lies on S, and satisfies in the water

$$\left(\frac{1}{c_o^2}\frac{\partial^2}{\partial t^2}-\nabla^2\right)G=\delta(\mathbf{x}-\mathbf{y})\delta(t-\tau)\quad\text{where } G=0 \text{ for } t<\tau.\tag{3}$$

Green's theorem and the radiation condition applied to Eqs. (1) and (3) then permit the pressure in the water to be expressed in the form [8,19–23]

$$p(\mathbf{x},t)=\oint_S\left(p(\mathbf{y},\tau)\frac{\partial G}{\partial y_n}(\mathbf{x},\mathbf{y},t-\tau)-G(\mathbf{x},\mathbf{y},t-\tau)\frac{\partial p}{\partial y_n}(\mathbf{y},\tau)\right)\mathrm{d}S(\mathbf{y})\,\mathrm{d}\tau\equiv\oint_S p(\mathbf{y},\tau)\frac{\partial G}{\partial y_n}(\mathbf{x},\mathbf{y},t-\tau)\,\mathrm{d}S(\mathbf{y})\,\mathrm{d}\tau,\tag{4}$$

where the integration is over all values of the source time $-\infty<\tau<+\infty$, and the surface integral is taken over the interface S (on which $G=0$) with the local normal coordinate y_n directed into the water.

2.2. The acoustic pressure frequency spectrum at high frequencies

When the frequency is sufficiently large that $k_oR>1$, where $k_o=\omega/c_o$ is the acoustic wavenumber of sound of radian frequency ω, the radiation field in the water is the same as that produced by impact of the jet on a plane interface $x_3=0$. Green's function then reduces to

$$G(\mathbf{x},\mathbf{y},t-\tau)=\frac{1}{4\pi|\mathbf{x}-\mathbf{y}|}\delta\left(t-\tau-\frac{|\mathbf{x}-\mathbf{y}|}{c_o}\right)-\frac{1}{4\pi|\mathbf{x}-\overline{\mathbf{y}}|}\delta\left(t-\tau-\frac{|\mathbf{x}-\overline{\mathbf{y}}|}{c_o}\right),\tag{5}$$

where $\overline{\mathbf{y}}=(y_1,y_2,-y_3)$ is the 'image' in the planar interface of the source point $\mathbf{y}$ in the water. $G(\mathbf{x},\mathbf{y},t-\tau)$ vanishes when either of x_3, y_3 lies on the interface.

The acoustic pressure fluctuations in the water are then given without further approximation by substituting from Eqs. (2) and (5) into Eq. (4), yielding the dipole formula

$$p(\mathbf{x},t)=-\frac{\partial}{\partial x_3}\left[\frac{1}{2\pi|\mathbf{x}|}F\left(t-\frac{|\mathbf{x}|}{c_o}\right)\right],\quad x_3>0.\tag{6}$$

The unsteady component of the jet impact force $F(t)$ may be regarded as stationary random in time with frequency spectrum

$$\Phi_{FF}(\omega)=\frac{1}{2\pi}\int_{-\infty}^{\infty}\langle F(t)F(t+\tau)\rangle\,\mathrm{e}^{\mathrm{i}\omega\tau}\,\mathrm{d}\tau,\tag{7}$$

where the angle brackets $\langle\ \rangle$ denote an ensemble or time average. It follows from Eq. (6) that the corresponding pressure frequency spectrum $\Phi_{pp}(\mathbf{x},\omega)$ at the far-field point $\mathbf{x}$ in the water is given by

$$\Phi_{pp}(\mathbf{x},\omega)=\Phi_{FF}(\omega)\left|\frac{\partial}{\partial x_3}\left(\frac{\mathrm{e}^{\mathrm{i}k_o|\mathbf{x}|}}{2\pi|\mathbf{x}|}\right)\right|^2\approx\frac{\cos^2\theta}{4\pi^2|\mathbf{x}|^2}\,k_o^2\Phi_{FF}(\omega),\quad|\mathbf{x}|\to\infty,\tag{8}$$

where $\cos\theta=x_3/|\mathbf{x}|$ defines the dipolar directional characteristics of the high frequency sound in the water.

2.3. The acoustic pressure frequency spectrum at low frequencies

In the opposite extreme in which the acoustic wavelength is larger than the overall length of the supercavity it is necessary to take explicit account of cavity geometry. The radiation excited by the jet in this case can be determined by modelling the shape of the cavity by a prolate ellipsoid of large aspect ratio, as indicated in Fig. 4. In the limit of low frequency Green's function $G(\mathbf{x},\mathbf{y},t-\tau)$ in the general solution (4) that vanishes on the ellipsoidal interface can be calculated in a tractable form only for an observer at $\mathbf{x}$ in the far field.

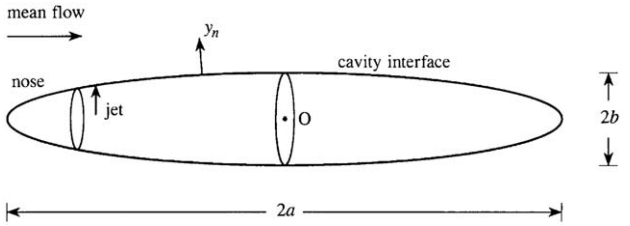

Fig. 4. Idealised ellipsoidal cavity interface used to estimate the low frequency sound radiated into the water from the jet.

Thus, for a general ellipsoid with semi-axes $a,\ b,\ c$, say, expressed in the conventional Cartesian form

$$\frac{x^2}{a^2}+\frac{y^2}{b^2}+\frac{z^2}{c^2}=1 \tag{9}$$

(where the coordinate origin is now shifted to the geometric centre O of the ellipsoid) we find [8,24,25]

$$G(\mathbf{x},\mathbf{y},t-\tau)\approx\frac{\mathcal{F}(\mathbf{y})}{4\pi|\mathbf{x}|}\delta\left(t-\tau-\frac{|\mathbf{x}|}{c_o}\right),\quad |\mathbf{x}|\to\infty, \tag{10}$$

where

$$\mathcal{F}(\mathbf{y})=\int_0^{\lambda(\mathbf{y})}\frac{\mathrm{d}\xi}{\sqrt{(a^2+\xi)(b^2+\xi)(c^2+\xi)}}\Bigg/\int_0^{\infty}\frac{\mathrm{d}\xi}{\sqrt{(a^2+\xi)(b^2+\xi)(c^2+\xi)}}, \tag{11}$$

and $\lambda(\mathbf{y})$ is the non-negative root of the equation

$$\frac{x'^2}{(a^2+\lambda)}+\frac{y'^2}{(b^2+\lambda)}+\frac{z'^2}{(c^2+\lambda)}=1\quad\text{where }\mathbf{y}=(x',y',z'). \tag{12}$$

The function $\mathcal{F}(\mathbf{y})$ vanishes when $\mathbf{y}$ lies on the ellipsoidal cavity interface (9), where $\lambda(\mathbf{y})\equiv 0$.

Hence, substituting from (10) into Eq. (4) and using the narrow jet approximation (2) (with obvious adjustments for the change in the coordinate system and cavity geometry), the acoustic pressure in the water at low frequencies is found to be given by

$$p(\mathbf{x},t)=\frac{\partial\mathcal{F}}{\partial y_n}\frac{F(t-|\mathbf{x}|/c_o)}{4\pi|\mathbf{x}|},\quad |\mathbf{x}|\to\infty, \tag{13}$$

where $\partial\mathcal{F}/\partial y_n$ is evaluated on the cavity interface at the point of impact of the jet. Eq. (13) represents the acoustic field of a monopole source, whose strength is determined by the volumetric fluctuations of the cavity produced by the unsteady jet-impact force.

For a prolate ellipsoid we put $b=c\ll a$, and take the major axis of the ellipsoid of length $2a$ to correspond to the streamwise length of the supercavity (as in Fig. 4). The jet impinges on the cavity interface just aft of the nose section, say at a distance $\sim 0.6a$ from the centroid of the ellipsoid. Then Eq. (13) reduces to

$$p(\mathbf{x},t)=\frac{F(t-|\mathbf{x}|/c_o)}{4\pi|\mathbf{x}|R\ln(2a/b)},\quad |\mathbf{x}|\to\infty, \tag{14}$$

and the corresponding acoustic pressure frequency spectrum becomes

$$\Phi_{pp}(\omega)\approx\frac{\Phi_{FF}(\omega)}{16\pi^2|\mathbf{x}|^2(R\ln(2a/b))^2}. \tag{15}$$

This approximation is nominally applicable for $k_oa<1$ or, because $R\sim 0.1a$, for $k_oR\ll 0.1$.

2.4. *The acoustic pressure at intermediate frequencies:* $0.1<k_oR<1$

The gap between the high and low frequency approximations of Sections 2.2 and 2.3 is occupied by sound waves satisfying $0.1<k_oR<1$. Such waves have wavelengths larger than the local cavity radius R, but smaller than the overall cavity length. A first approximation for the sound generated by the jet in this case is obtained by modelling the cavity interface close to the jet as a circular cylinder of radius R (Fig. 5). The cylinder is nominally infinitely long, but its effective dynamical length $\sim O(1/k_o)$, which is small compared to the overall length of the supercavity.

In this case the leading order approximation to the acoustic Green's function (which vanishes on the cylindrical interface and is calculated by the method described in [8]) can be cast in the form

$$G(\mathbf{x},\mathbf{y},t-\tau)\approx\frac{1}{8\pi^2|\mathbf{x}|}\int_{-\infty}^{\infty}\left(1-\frac{\mathrm{H}_0^{(1)}(k_or\sin\vartheta)}{\mathrm{H}_0^{(1)}(k_oR\sin\vartheta)}\right)\mathrm{e}^{-\mathrm{i}\omega(t-\tau-|\mathbf{x}-x'\mathbf{i}|/c_o)}\,\mathrm{d}\omega,\quad |\mathbf{x}|\to\infty, \tag{16}$$

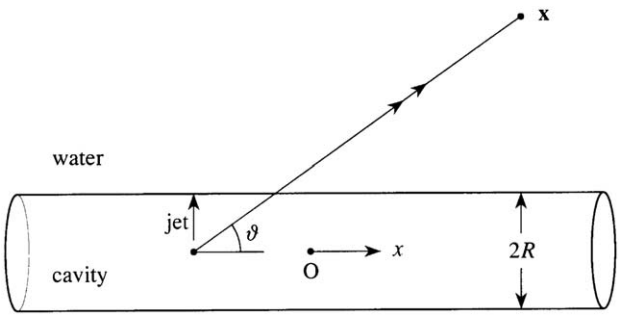

Fig. 5. Cylindrical cavity used to estimate acoustic pressure at intermediate frequencies.

where $\mathbf{y}=(x',y',z')$, $r=\sqrt{y'^2+z'^2}$ and $\mathbf{i}$ is a unit vector in the axial (x) direction. The angle $\vartheta=\cos^{-1}(x/|\mathbf{x}|)$ is indicated in Fig. 5, and represents the direction between the positive x-axis and the observer in the far field.

It follows, as before by substitution into (4), that

$$p(\mathbf{x},t)\approx\frac{1}{4\pi|\mathbf{x}|}\int_{-\infty}^{\infty}k_o\hat{F}(\omega)\,\frac{\sin\vartheta\,\mathrm{H}_1^{(1)}(k_oR\sin\vartheta)}{\mathrm{H}_0^{(1)}(k_oR\sin\vartheta)}\,\mathrm{e}^{-\mathrm{i}\omega(t-|\mathbf{x}|/c_o)}\,\mathrm{d}\omega,\quad |\mathbf{x}|\to\infty, \tag{17}$$

where $\hat{F}(\omega)=(1/2\pi)\int_{-\infty}^{\infty}F(\tau)\mathrm{e}^{\mathrm{i}\omega\tau}\,\mathrm{d}\tau$ and the coordinate origin has been shifted to the location of the jet on the cylinder axis, and therefore that

$$\Phi_{pp}(\omega)\approx\frac{\Phi_{FF}(\omega)k_o^2\sin^2\vartheta}{16\pi^2|\mathbf{x}|^2}\left|\frac{\mathrm{H}_1^{(1)}(k_oR\sin\vartheta)}{\mathrm{H}_0^{(1)}(k_oR\sin\vartheta)}\right|^2,\quad 0.1<k_oR<1. \tag{18}$$

2.5. Spectrum of the acoustic power radiated into the water

In the high frequency approximation of Section 2.2 the spectrum $\Pi(\omega)$ of the acoustic power radiated into the water from the jet impact with the cavity interface is given in terms of $\Phi_{pp}(\omega)$ by

$$\Pi(\omega)=\int_0^{2\pi}\int_0^{\pi/2}\frac{\Phi_{pp}(\omega)}{\rho_oc_o}|\mathbf{x}|^2\sin\theta\,\mathrm{d}\theta\,\mathrm{d}\phi,\quad |\mathbf{x}|\to\infty, \tag{19}$$

where $\Phi_{pp}(\omega)$ is given by Eq. (8) and the integration is over the surface of a large hemisphere of radius $|\mathbf{x}|$ in the water, centred at the origin at the centroid of the impact region. The power radiated by the omnidirectional, low frequency monopole of Section 2.3 is equal to the limiting value of $4\pi|\mathbf{x}|^2\Phi_{pp}(\omega)/\rho_oc_o$ as $|\mathbf{x}|\to\infty$, where $\Phi_{pp}(\omega)$ is given by Eq. (15). At intermediate frequencies the power is given by an integral of the type (19) with the θ integration replaced by an integral with respect to ϑ over $0<\vartheta<\pi$ and $\Phi_{pp}(\omega)$ defined by Eq. (18).

Collecting together the results of these various calculations, we find

$$\Pi(\omega)\sim\begin{cases}\dfrac{k_o^2\Phi_{FF}(\omega)}{6\pi\rho_oc_o}, & k_oR>1,\\[2ex] \dfrac{k_o^2\mathcal{Z}(k_oR)\Phi_{FF}(\omega)}{6\pi\rho_oc_o}, & 0.1<k_oR<1,\\[2ex] \dfrac{\Phi_{FF}(\omega)}{4\pi\rho_oc_oR^2\ln^2(2a/b)}, & k_oR<0.1,\end{cases} \tag{20}$$

where

$$\mathcal{Z}(k_oR)=\frac{3}{4}\int_0^{\pi}\sin^3\vartheta\left|\frac{\mathrm{H}_1^{(1)}(k_oR\sin\vartheta)}{\mathrm{H}_0^{(1)}(k_oR\sin\vartheta)}\right|^2\mathrm{d}\vartheta. \tag{21}$$

Observe that $k_o^2\mathcal{Z}(k_oR)\sim 1/R^2\ln^2(k_0R)$ as $k_oR\to 0$, which mimics the behaviour of the low frequency approximation with a replaced by $1/k_o$ and b replaced by R. Similarly, $\mathcal{Z}(k_oR)\approx 1$ when $k_oR\gg 1$, so that the high and intermediate frequency approximations are then the same.

These formulae are used below in Section 4.

3. Frequency spectrum of the jet impact force

Measurements of the unsteady surface force produced by low speed jet impact on a nominally a rigid wall have been made by Foley [11] at ARL for one of the jets issuing from the gas injector ring of the supercavitating vehicle of Fig. 1. The radius of the injector ring is 25 mm and the ring is centred on the axis of symmetry of the vehicle. Each of the 20 equally spaced and radially directed jet nozzles has an exit diameter $D_o = 3.2$ mm, and was supplied with compressed air by means of a gas line passing through the vehicle mounting strut. The experiment was performed by mounting the vehicle on a laboratory bench with the cavitator removed, and the test jet was isolated by plugging the four nearest neighbour nozzles, two on either side of the test nozzle. The test jet was directed at normal incidence onto the plane measurement surface of a dynamic force transducer which was firmly attached to a massive aluminum yoke to reduce the influence of structural vibrations (details of the experiment are discussed in [11]). The impact force spectrum was measured for gas volume flow rates $Q \approx 0.0047$, 0.0071, 0.0094 SCMS (standard cubic metres per second) and for a range of jet lengths between $\ell = 15$ and 45 mm. In typical supercavity water tunnel tests at ARL the volume flow rate $Q \sim 0.0094$ SCMS and $\ell \sim 35$ mm, and the following discussion is confined to jets of this length.

The jet impact diameter D is estimated by assuming that the turbulent jet grows conically, with total angle of spread equal to 25° [22,26], i.e. $D \approx D_o + 0.44\ell = 18.6$ mm. Similarity would normally permit the effective centreline jet speed U at the wall to be approximated by [22,26]

$$U \approx 3U_o \frac{\ell}{D_o}\left(\frac{D_o}{D}\right)^2. \tag{22}$$

However, the length $\ell \simeq 11D_o$ of the jet is probably too short for self-similarity to be attained at the interface, and according to Hinze [26, Section 6.11] the effective impact velocity U should not differ significantly from U_o. Actually, Eq. (22) predicts $U/U_o \simeq 0.97$, and we shall therefore assume in what follows that $U = U_o$. The measured values of U_o, U are given in Table 1 for $\ell = 35$ mm and $D = 18.6$ mm.

Similarity would also imply, for appropriately defined impact values of D and U, that the force spectrum normalised by $F_o^2 = (\rho_A U^2)^2(\pi/4D^2)^2$ should be a universal function of $\omega D/U$, where F_o is the nominal mean force exerted by the jet on the wall, $\rho_A = 1.2$ kg/m^3 being the mean density of the jet. Foley's [11] measurements indicate that $\Phi_{FF}(\omega)$ decays like $\omega^{-5/2}$ at high frequencies, and that it is well approximated by the empirical formula

$$\frac{\Phi_{FF}(\omega)U}{F_o^2 D} = \frac{\alpha}{(1+\varepsilon^2(\omega D/U)^2)^{5/4}}, \tag{23}$$

where α and ε are constants. This formula recognises the fact that the contribution to the surface force from turbulence pressure fluctuations of characteristic scale U/ω decreases rapidly when $U/\omega < D$. It is found that this decrease is well represented by taking $\varepsilon = 1.6$ in (23).

Fig. 6 shows plots of the approximation (23) for Foley's [11] experimental results for the three cases in Table 1 (which also lists the corresponding values of α). In all cases $\varepsilon = 1.6$ and the coefficient α has been adjusted to give the best agreement with the data. The small, but evident differences in the measured spectral levels presumably represent the departure from similarity.

3.1. Measurements of Strong et al.

These results may be compared with measurements of the jet impact wall pressure made by Strong et al. [17]. One of their experiments involved an air jet exhausting at speed $U_o = 41.5$ m/s from a circular nozzle of diameter $D_o = 102$ mm and directed at normal incidence onto a heavy plate at distance $\ell = 7D_o$. The space–time correlation of the unsteady surface pressure on the plate at frequencies between 40 and 10,000 Hz was measured using two flush mounted pinhole microphones, one at the centroid of the impact area and the second at varying distances from the centroid. In particular, they measured the wall pressure frequency spectrum $\Phi_J(\omega)$ at the centroid shown in Fig. 7 (•••).

There is no direct relation between the 'point' pressure spectrum $\Phi_J(\omega)$ and the spectrum $\Phi_{FF}(\omega)$ of the overall force exerted on the plate. However, an approximate effective force spectrum can be defined in terms of $\Phi_J(\omega)$ by introducing a surface pressure 'correlation area' $\mathcal{A}$, say, in terms of which

$$\Phi_{FF}(\omega) \approx \Phi_J(\omega)\frac{\pi}{4}D^2\mathcal{A}, \quad \mathcal{A} < \frac{\pi}{4}D^2. \tag{24}$$

Table 1
Overall volume flow rates and velocities when $\ell = 35$ mm and $D = 18.6$ mm.

Q (SCMS)	U_o, U (m/s)	α, Eq. (23)
0.0047	27.1	17.28
0.0071	40.7	20.00
0.0094	54.2	26.61

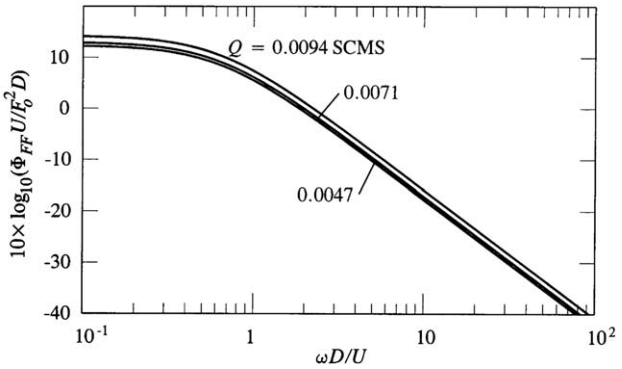

Fig. 6. Representation of the impact force spectra measured by Foley [11] by the similarity formula (23) for volume flow rates $Q = 0.0047$, 0.0071, 0.0094 SCMS when $\ell = 35$ mm, $D_o = 3.2$ mm. See Table 1.

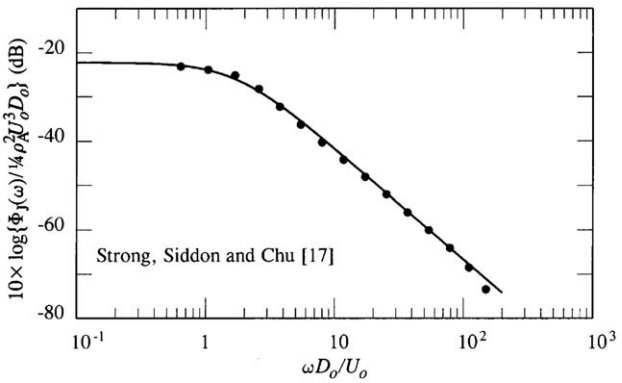

Fig. 7. Point wall pressure spectrum (•••) at the centroid of the jet impact region measured by Strong et al. [17] and the empirical approximation (25) (——) for $\ell = 7D_o$, $U_o = 41.5$ m/s.

The length $\ell = 7D_o$ of the jet investigated by Strong et al. [17] is too short for the jet to be self-similar near the wall [26]. Indeed, the effective impact velocity U is unlikely to differ significantly from its nozzle exit value U_o. However, the measured pressure spectrum in Fig. 7 clearly decays roughly like $\omega^{-5/2}$ at high frequencies, so that Eq. (24) appears to justify the use of the following empirical representation of the form (23):

$$\frac{\Phi_J(\omega)}{(\frac{1}{4}\rho_A^2 U_o^3 D_o)} = \frac{\alpha'}{(1+\varepsilon^2(\omega D_o/U_o)^2)^{5/4}}. \tag{25}$$

This is plotted as the solid line curve (——) in Fig. 7 for $\alpha' = 0.006$, $\varepsilon = 0.6$.

4. Sound radiated into the water

4.1. Spectrum for $Q = 0.0047$ SCMS

The relations (20) and (23) permit the spectrum of the overall acoustic power radiated into the water from the impact region to be expressed in the forms

$$\frac{\Pi(\omega)\rho_o c_o UD}{F_o^2} = \frac{\alpha (D/R)^2}{4\pi \ln^2(2a/b)(1+\varepsilon^2(k_oD/M)^2)^{5/4}}, \quad k_oR<0.1, \tag{26a}$$

$$= \frac{\alpha (k_oD)^2 \mathcal{Z}(k_oR)}{6\pi(1+\varepsilon^2(k_oD/M)^2)^{5/4}}, \quad 0.1<k_oR<1, \tag{26b}$$

$$= \frac{\alpha (k_oD)^2}{6\pi(1+\varepsilon^2(k_oD/M)^2)^{5/4}}, \quad k_oR>1, \tag{26c}$$

where M is the jet Mach number U/c_o relative to the speed of sound in water. These approximations are shown plotted against k_oD (——) over their respective ranges of validity in Fig. 8 for the experimental case where $\ell = 35$ mm and

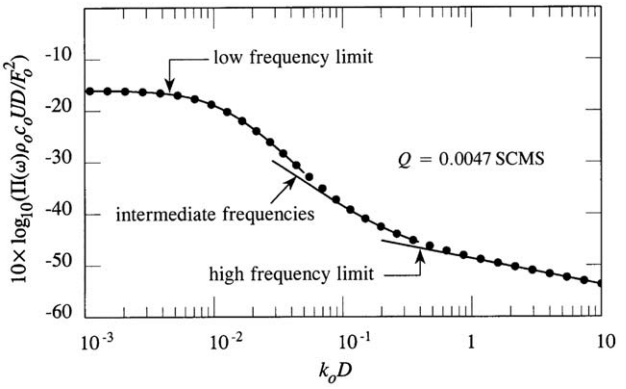

Fig. 8. Low, intermediate and high frequency approximations (——) defined in (26a)–(26c) for the acoustic power spectrum when $Q = 0.0047$ SCMS, $\ell = 35$ mm, $D_o = 3.2$ mm. See Table 1. The dotted curve (•••) is the smoothly varying interpolation defined by Eq. (27) for $s = 5$.

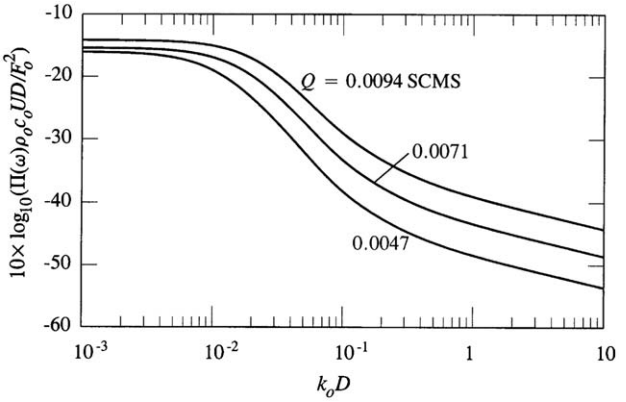

Fig. 9. Interpolated acoustic power spectra defined by Eq. (27) for $s = 5$ of the sound radiated into the water produced by the impact of a single jet on the cavity interface, for volume flow rates $Q = 0.0047,\ 0.0071,\ 0.0094$ SCMS when $\ell = 35$ mm, $D_o = 3.2$ mm and $b/a = 0.2$.

$Q = 0.0047$ SCMS (so that $R/D = 60/18.6 \approx 3.2$), and where in the low frequency approximation it is assumed for the prolate ellipsoid that $b/a = 0.2$.

The three approximating curves are seen to provide consistent and regular variations in $\Pi(\omega)$ over the whole frequency range. It is eminently reasonable, therefore, to adopt for practical purposes the interpolated spectrum shown dotted (•••) in the figure. A simple formula for this curve is obtained by first recalling that $\mathcal{Z}(k_oR) \approx 1$ for $k_oR > 1$, so that the intermediate and high frequency approximations automatically merge near $k_oR = 1$. Then over the whole frequency range we can take for the interpolated spectrum

$$\frac{\Pi(\omega)\rho_o c_o UD}{F_o^2} \approx \frac{\alpha}{6\pi(1+\varepsilon^2(k_oD/M)^2)^{5/4}} \left\{ ((k_oD)^2\mathcal{Z}(k_oR))^s + \left(\frac{3(D/R)^2}{2\ln^2(2a/b)}\right)^s \right\}^{1/s}, \tag{27}$$

where the free parameter $s > 1$. For the dotted curve in Fig. 8 we have taken $s = 5$.

4.2. Interpolated spectra

Eq. (27) can be used to define interpolated acoustic power spectra for all of the experimental conditions of Table 1, with corresponding force spectra displayed in Fig. 6, i.e. for $Q = 0.0047,\ 0.0071,\ 0.0094$ SCMS, $\ell = 35$ mm, $R = 60$ mm and $b/a = 0.2$. These are plotted in Fig. 9.

The peak radiation occurs at the lower frequencies, where the acoustic wavelength is comparable to the cavity cross-sectional diameter or larger. The high frequency sound is typically 20–30 dB weaker, and decays relatively slowly like $(k_oD)^{-1/2}$. However, the detailed predictions for $k_oD \gg 1$, must be regarded as tentative, because the acoustic wavelength then becomes smaller than the diameter D of the jet impact region on the cavity interface. Therefore, phase interference between sound generated at different points within the impact region (which is neglected in the approximation in which

the jet cross-section is taken to be infinitesimal) is likely to reduce further the predicted acoustic power, which would then tend to decay more rapidly with increasing frequency.

5. Conclusion

Foley et al. [10] and Foley [11] postulated that the principal characteristics of the sound produced in water by a turbulent gas jet impinging on the interface of a supercavity could be expressed in terms of the overall unsteady force exerted on the interface by the jet. They introduced an analogy whereby the force spectrum was identified with that which the same jet would produce when incident on a rigid wall. Measurements of this force could then be used in the acoustic equations to predict the radiated sound. Foley's [11] original analysis treated this acoustic problem by assuming the frequency to be sufficiently large that the cavity interface could always be regarded as locally flat. It was recognised, however, that the measured force fluctuations contained significant energy at low frequencies, and that a direct extrapolation of acoustic predictions to the model scale supercavitating vehicle under test at ARL actually reveals substantial acoustic energy at frequencies that are sufficiently low that the plane interface approximation is not valid.

The theoretical analysis in this paper confirms the importance of the low frequency domain ($k_oR<1$), which is predicted to dominate the radiation produced by the impact of the jet on the interface. Our results indicate the existence of a similarity analytical formula for the surface force spectrum for the data presented in this paper, and also for other experimental data acquired by Foley [11] but not reported here. This formula has been used to predict the acoustic radiation at low, high and intermediate frequencies and furnishes a smoothly varying interpolated representation of the power spectrum over the whole frequency range. A single jet impinging on the interface produces sound of monopole type ('omnidirectional' in the water) when k_oR is less than about 0.1. At higher frequencies ($k_oR>1$) the acoustic field has the directivity of a dipole, with dipole axis parallel to the axis of the jet, provided the latter impinges on the interface at near normal incidence.

For an array of statistically independent coplanar jets distributed uniformly around the gas injector ring of the ARL vehicle, the directivity of the sound radiated from the supercavity will be omnidirectional when $k_oR<0.1$. For increasingly higher frequencies, however, the dipole characteristic will tend progressively to confine the sound to a near-planar, circularly symmetric region centred on the common plane of the jet axes at right angles to the principal axis of the vehicle.

Acknowledgements

This work was sponsored by the Office of Naval Research Code 333, Grant N000014-06-1-0270 under the University/Laboratory Initiative directed by Dr. Kam W. Ng.

References

[1] C.E. Brennen, *Cavitation and Bubble Dynamics*, Oxford University Press, Oxford, 1995.
[2] J.P. Franc, J.M. Michel, *Fundamentals of Cavitation*, Kluwer Academic Publishers, Dordrecht, 2004.
[3] R. Kuklinski, C. Henoch, J. Castano, Experimental study of ventilated cavities on dynamic test model, Paper presented at *Cav2001*: *Session B3.004*, 2001.
[4] E. Silberman, C.S. Song, Instability of ventilated cavities, *Journal of Ship Research* 5 (1) (1961) 13–33.
[5] C.S. Song, Pulsation of ventilated cavities, *Journal of Ship Research* 5 (4) (1962) 8–20.
[6] M.J. Lighthill, On sound generated aerodynamically. Part I: general theory, *Proceedings of the Royal Society of London A* 211 (1952) 564–587.
[7] W.K. Blake, *Mechanics of Flow-induced Sound and Vibration*, Academic Press, New York, 1986.
[8] M.S. Howe, *Acoustics of Fluid–Structure Interactions*, Cambridge University Press, Cambridge, 1998.
[9] S.D. Young, T.A. Brungart, G.C. Lauchle, M.S. Howe, Effect of a downstream ventilated gas cavity on the spectrum of turbulent boundary layer wall pressure fluctuations, *Journal of the Acoustical Society of America* 118 (2005) 3506–3512.
[10] A.W. Foley, M.S. Howe, T.A. Brungart, Sound generated by gas-jet impingement on the interface of a supercavity, *Proceedings of IMECE2008*, *2008 ASME International Mechanical Engineering Congress and Exposition*, November 2–6, 2008, Boston, MA, USA.
[11] A.W. Foley, *Investigations of the Sound Generated by Supercavity Ventilation*, PhD Thesis, Department of Mechanical Engineering, Boston University, 2009.
[12] J. Shen, W.C. Meecham, Quadrupole directivity of jet noise associated when impinging on normal plates, *Journal of the Acoustical Society of America* 94 (1993) 1415–1424.
[13] W.A. Olsen, J.H. Miles, R.G. Dorsch, Noise generated by the impingement of a jet upon a large flat board, *NASA*, 1972, TN D-7075.
[14] C.-Y. Kuo, A.P. Dowling, Acoustics of a two-dimensional compact jet impinging normally onto a flat plate, *Journal of Fluid Mechanics* 414 (2000) 251–284.
[15] A. Powell, Aerodynamic noise and the plane boundary, *Journal of the Acoustical Society of America* 32 (1960) 962–990.
[16] A. Powell, Nature of the sound sources in low-speed jet impingement, *Journal of the Acoustical Society of America* 90 (1991) 3326–3331.
[17] D.R. Strong, T.E. Siddon, W.T. Chu, Pressure fluctuations on a flat plate with oblique jet impingement, National Aeronautics and Space Administration Contractor Report, 1967, CR-839.
[18] A.W. Foley, M.S. Howe, T.A. Brungart, Sound generated by a jet-excited spherical cavity, *Journal of Sound and Vibration* 315 (2008) 88–99.
[19] A.D. Pierce, *Acoustics, An Introduction to its Principles and Applications*, American Institute of Physics, New York, 1989.
[20] M.C. Junger, D. Feit, *Sound, Structures and their Interactions*, Acoustical Society of America, New York, 1993.
[21] B.B. Baker, E.T. Copson, *The Mathematical Theory of Huygens' Principle*, second ed., Oxford University Press, Oxford, 1969.
[22] L.D. Landau, E.M. Lifshitz, *Fluid Mechanics*, second ed., Pergamon, Oxford, 1987.
[23] D.G. Crighton, A.P. Dowling, J.E. Ffowcs Williams, M. Heckl, F.G. Leppington, in: *Modern Methods in Analytical Acoustics* (*Lecture Notes*), Springer, London, 1992.
[24] H. Lamb, *Hydrodynamics*, sixth ed., Cambridge University Press, Cambridge, 1932.
[25] H. Bateman, *Partial Differential Equations of Mathematical Physics*, Dover Publications, New York, 1944.
[26] J.O. Hinze, *Turbulence*, second ed., McGraw-Hill, New York, 1975.